Cross sections for energy transfer in collisions between two excited sodium atoms

J. Huennekens and A. Gallagher*
Joint Institute for Laboratory Astrophysics, University of Colorado and National Bureau of Standards, Boulder, Colorado 80309
(Received 26 July 1982)

We have measured cross sections, σ_{nL}, for the excitation transfer process $Na(3P)+Na(3P)\rightarrow Na(3S)+Na(nL)$, where nL is the $4D$ or $5S$ level. Our results are $\sigma_{4D}=23$ Å$^2\pm35\%$ and $\sigma_{5S}=16$ Å$^2\pm35\%$ at $T\sim600$ K. To obtain these cross sections we have used pulsed excitation and measured the intensities of $4D$, $5S$, and $3P$ fluorescence emissions, and the spatial distribution of excited atoms resulting from radiation diffusion, as well as the excited atom density as a function of time. Additionally, we have accounted for (time-dependent) radiation trapping of $3P$ and nL level radiation and for the resulting anisotropies of these fluorescence emissions. Comparisons of our results with theory have been made, and their relevance to other experiments is discussed.

I. INTRODUCTION

When sodium vapor is optically excited to the $3P$ state, fluorescence can be detected from higher energy levels, particularly those whose energy is close to twice the $3P$ energy. Allegrini *et al.*[1] were the first to report observations of this and to attribute the excitation of the higher levels to collisions between two excited atoms. The energy-transfer process can be represented by the expression

$$Na(3P)+Na(3P)\xrightarrow{k_{nL}}Na(3S)+Na(nL)\ , \qquad (1)$$

where $Na(nL)$ is sodium in a state lying higher than $3P$, and k_{nL} is the rate coefficient for the reaction.

One reason for interest in these rate coefficients is that they can be related to long-range alkali-alkali interactions that should be calculable. Another is that this process followed by photoionization or collisional ionization is an important mechanism for producing the seed electrons that trigger runaway ionization of resonantly excited, high-density metal vapors, as was first observed by Lucatorto and McIlrath.[2] Models of laser driven ionization, such as those of Measures[3] and Victor and Lafyatis[4] are sensitive to cross sections for the "energy pooling" processes represented by Eq. (1). In addition, Müller and Hertel[5] report lasing in the $5S\rightarrow4P$ transition, following excitation of the $3P$ level, indicating that these energy pooling processes may be of interest in this context as well.

Many difficulties complicate a measurement of the rate coefficients, k_{nL}. For example, when strong excitation is used, radiation trapping by $Na(3P)$ atoms attenuates $nL\rightarrow3P$ radiation and changes branching ratios of the higher levels. Additionally, an accurate knowledge of the spatial distribution and absolute value of the $3P$ atom density is needed. Previous measurements[6,7] of these rate coefficients have not adequately accounted for these effects, and they disagree by several orders of magnitude. The experiment being described here overcomes these difficulties by directly measuring the absolute value and the spatial and time dependences of the $3P$ atom density, by reducing the optical measurements to intensity ratio measurements, and by correcting for changes in branching ratios.

Figure 1 shows the relevant sodium energy levels. In this experiment we studied only the processes which populate the $4D$ and $5S$ levels, which are separated from the initial energy of two $3P$ atoms by

$$\Delta E_{nL}\equiv E_{nL}-2E_{3P}\ .$$

These two levels lie within $|\Delta E|=800$ cm^{-1} and are therefore more likely to be populated by process (1) than are other, more distant levels. The $4F$ level also lies as close, but k_{4F} was not measured owing to the long wavelength of the $4F$-state emission. However, we will say more about the probable contributions of the $4F$ level later. The $5P$ level lies at $\Delta E\cong1100$ cm^{-1}, but radiation from this level was also not measured. Fluorescence from the $6S$ and $5D$ levels, which have the next smallest $|\Delta E|$'s, was observed, but the signals were so weak that we can only put an upper bound on k_{6S} and k_{5D}. Rate coefficients for production of these and other high-lying levels can be obtained from our absolute values of k_{4D} and k_{5S}, and measurements of relative intensities such as those presented in Ref. 1.

To explain the basic idea of the experiment we consider here a simple model for the measured ratio of $4D\rightarrow3P$ to $3P\rightarrow3S$ fluorescence. In Fig. 1 we

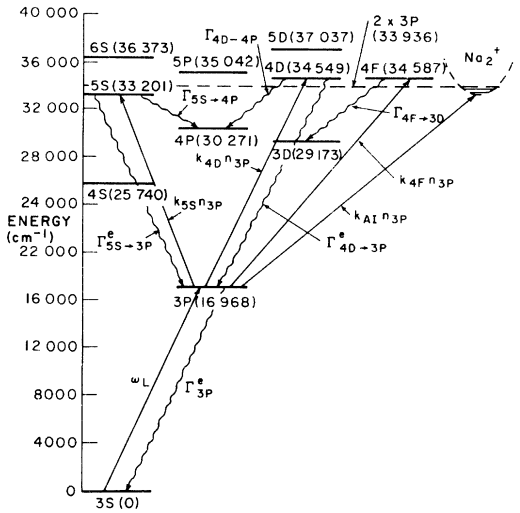

FIG. 1. Relevant collisional and radiative rates in the study of excited-atom–excited-atom collisions in sodium vapor. The energy of two Na($3P$) atoms is indicated by a dashed line; all other energies are Na(nL)+Na($3S$) relative to Na($3S$)+Na($3S$). Energies are given in cm^{-1} (from Ref. 8). Na_2^+ potential from Ref. 9.

have described both the $3P\rightarrow 3S$ and $4D\rightarrow 3P$ fluorescence by effective radiative decay rates Γ^e due to radiation trapping (we define natural radiative rates as $\Gamma_{nL\rightarrow n'L'}$ and trapped effective rates as $\Gamma^e_{nL\rightarrow n'L'}$). The $4D$ level is populated at a rate (per unit volume) $k_{4D}n_{3P}^2$ and decays at the rate $n_{4D}\Gamma^e_{4D}$ (where $\Gamma^e_{4D}\equiv\Gamma_{4D\rightarrow 4P}+\Gamma^e_{4D\rightarrow 3P}$). The $3P$ level decays at a rate $\Gamma^e_{3P}\ll\Gamma^e_{4D}$ so that $n_{4D}(t)$ essentially follows the instantaneous production rate yielding the quasisteady-state solution

$$\Gamma^e_{4D}n_{4D}(t)\cong k_{4D}[n_{3P}(t)]^2 . \tag{2}$$

Thus the ratio of the $4D\rightarrow 3P$ to $3P\rightarrow 3S$ fluorescence intensities at the time t is

$$\frac{I_{4D\rightarrow 3P}(t)}{I_{3P\rightarrow 3S}(t)}=\frac{\Gamma^e_{4D\rightarrow 3P}n_{4D}(t)}{\Gamma^e_{3P}n_{3P}(t)}\frac{\hbar\omega_{4D\rightarrow 3P}}{\hbar\omega_{3P\rightarrow 3S}}$$
$$\cong\frac{\Gamma^e_{4D\rightarrow 3P}k_{4D}n_{3P}(t)}{\Gamma^e_{4D}\Gamma^e_{3P}}\frac{\omega_{4D\rightarrow 3P}}{\omega_{3P\rightarrow 3S}} , \tag{3}$$

where the ω's are the transition frequencies and where Eq. (2) has been used in the final step. Equation (3) can be solved for k_{4D} to yield

$$k_{4D}\cong\frac{I_{4D\rightarrow 3P}(t)}{I_{3P\rightarrow 3S}(t)}\frac{\Gamma^e_{4D}}{\Gamma^e_{4D\rightarrow 3P}}\frac{\Gamma^e_{3P}}{n_{3P}(t)}\frac{\omega_{3P\rightarrow 3S}}{\omega_{4D\rightarrow 3P}} . \tag{4}$$

In this experiment we have measured this intensity ratio, Γ^e_{3P} and $n_{3P}(t)$. Combined with calculated values of Γ^e_{4D} and $\Gamma^e_{4D\rightarrow 3P}$, this yields the desired rate coefficient. In Sec. IV, we will consider several complications to this simple picture.

II. THE EXPERIMENT

Figure 2 is a block diagram of the experimental setup. The sodium cell is a 5-cm stainless-steel block drilled out to make a cross and vacuum sealed with metal O-rings to sapphire windows. Only the hollow cross containing the Na vapor is shown in Fig. 2. As indicated, two arms of the cross contain sapphire rods which reduce the optical depth in the detection direction. The sodium vapor pressure is controlled by the temperature of a side arm, which is stabilized at typically 25–50 °C below the temperature of the cell. Sodium vapor pressure as a function of temperature reading was calibrated at low density by measurement of k_0, the line center absorption coefficient, and at high density by measurement of k_ν, the wing absorption coefficient, combined with an independent measurement of the self-broadening rate for the resonance lines (see Ref. 10). Vapor pressures obtained in this manner were 2–13 % above Nesmeyanov's[11] relationships.

The vapor is excited by a nitrogen-laser pumped dye laser (laser 1 in Fig. 2), of spectral width ~ 0.5 cm^{-1}, which is tuned to the D_2 ($3S_{1/2}$-$3P_{3/2}$) resonance line and which emits ~ 60 μJ in pulses of ~ 5-ns duration. Neutral density filters were used to study power dependences.

According to Holstein's theory[12] of radiation trapping, the excited-atom spatial distribution as a function of time can be expanded in eigenmodes as

$$n_e(\vec{r},t)=\sum_i c_i n_i(\vec{r})e^{-\beta_i t} . \tag{5}$$

The slowest decaying eigenvalue β_1 is called the fundamental-mode decay rate Γ^e. We have used a laser beam diameter of ~ 5 mm (see Fig. 3) in order

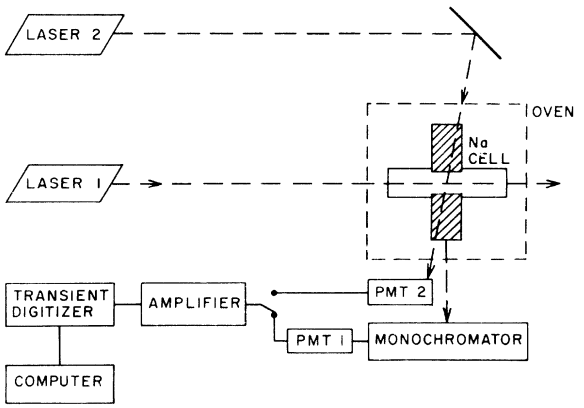

FIG. 2. Block diagram of the experimental setup. Sapphire rods inside the cell are indicated by cross hatching. PMT, photomultiplier.

to fill $\sim 80\%$ of the window gap and thereby maximize the overlap of the beam with this fundamental-mode excited atom spatial distribution (see Refs. 12 and 13). This minimizes the time required for the trapped fluorescence to reach a single-exponential decay rate.

Fluorescence is detected at right angles to the laser beam with a $\frac{3}{4}$-m double monochromator and a photomultiplier with an S-20 cathode response. The photomultiplier output is amplified, processed by a fast transient digitizer, and the time-resolved signals are stored on computer for later analysis. The imaging is such that we collect light from a thin strip of height ~ 5 mm oriented in the vertical direction (the region between the dashed lines in Fig. 3).

Figures 4(a) and 4(b) show typical time-resolved fluorescence signals averaged over 64 laser pulses. Figure 4(a) displays the total $4D \rightarrow 3P$ fluorescence signal $I_{4D\rightarrow 3P}(t)$ as well as its two spectral components $I_{4D_{5/2,3/2}\rightarrow 3P_{3/2}}(t)$ and $I_{4D_{3/2}\rightarrow 3P_{1/2}}(t)$. Note that the latter signal is initially larger due to the smaller amount of trapping of this component. This is due to initially smaller $n_{3P_{1/2}}$ following pulsed excitation of the $3P_{3/2}$ state. Figure 4(b) shows the total $3P \rightarrow 3S$ fluorescence $I_{3P}(t)$ and its two spectral components $I_{D_1}(t)$ and $I_{D_2}(t)$.

Laser 2 in Fig. 2 is a highly attenuated single-mode cw dye laser, tuned to the wings of the D_2 resonance transition. The cw beam, of diameter ~ 1.5 mm, crosses the pulsed-laser beam essentially at a right angle and is used to obtain the fraction of atoms in the $3P$ state as a function of time. Figure 4(c) shows a cw transmission signal averaged over 64 laser pulses by the transient digitizer. The intensity zero was obtained by blocking the cw laser, which also allowed us to measure the fluorescence background created by the N_2-laser pulse.

III. EXCITED-ATOM DENSITY MEASUREMENT

The cw transmission depends upon

$$\bar{n}_2(0,t) - \frac{g_0}{g_2}\bar{n}_0(0,t) ,$$

where the subscripts 2 and 0 refer to the $3P_{3/2}$ and $3S_{1/2}$ levels, respectively (the subscript 1 will be used for the $3P_{1/2}$ level), and where $\bar{n}_i(y,t)$ is the column density of n_i across the cell ($x=0$ to L) at the indicated value of y (see Fig. 3):

$$\bar{n}_i(y,t) \equiv \frac{1}{L}\int_0^L n_i(x,y,t)\,dx . \tag{6}$$

Thus measurement of the change in transmission of the cw laser as a function of time, combined with the known total Na density, yields the time-resolved $3P$-atom column density. Note that any velocity selection by the pump laser does not affect this measurement since the atomic velocities in the x and z directions are independent. However, the cw laser is tuned in the wing of the D_2 line and any hyperfine pumping would affect its transmission. Since the pulsed laser is spectrally much broader than the hyperfine splitting, this is not expected to occur here, and measurements with the cw laser tuned to opposite wings of the line confirmed this.

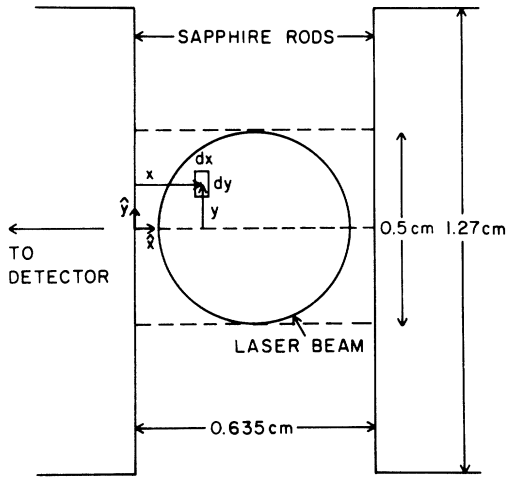

FIG. 3. Cross section of the center of the cell in the plane of the detection optics (a vertical plane through the sapphire rods in Fig. 2). This is defined as the x,y plane. The laser beam diameter of ~ 5 mm is depicted by the circle. We detect light from the 5-mm high region between the dashed lines and a thin slice in the z direction.

Before the pulsed laser fires, the ratio of the transmitted cw intensity I' to the intensity in the absence of absorption I_0 (obtained by tuning the cw laser far from resonance) is given by

$$\frac{I'}{I_0} = \exp\left[-n\left[\frac{k_\nu}{n}\right]L\right] , \tag{7}$$

where n is the total Na density and k_ν/n is independent of relative level populations (note the self-broadening rate is independent of whether the perturbers are in the ground or excited state).

Similarly, after the pulsed laser fires, the transmitted intensity $I(t)$ is given by

$$I(t)/I_0 = \exp\left[\left[-\bar{n}_0(0,t)+\bar{n}_2(0,t)\frac{g_0}{g_2}\right]\left[\frac{k_\nu}{n}\right]L\right] . \tag{8}$$

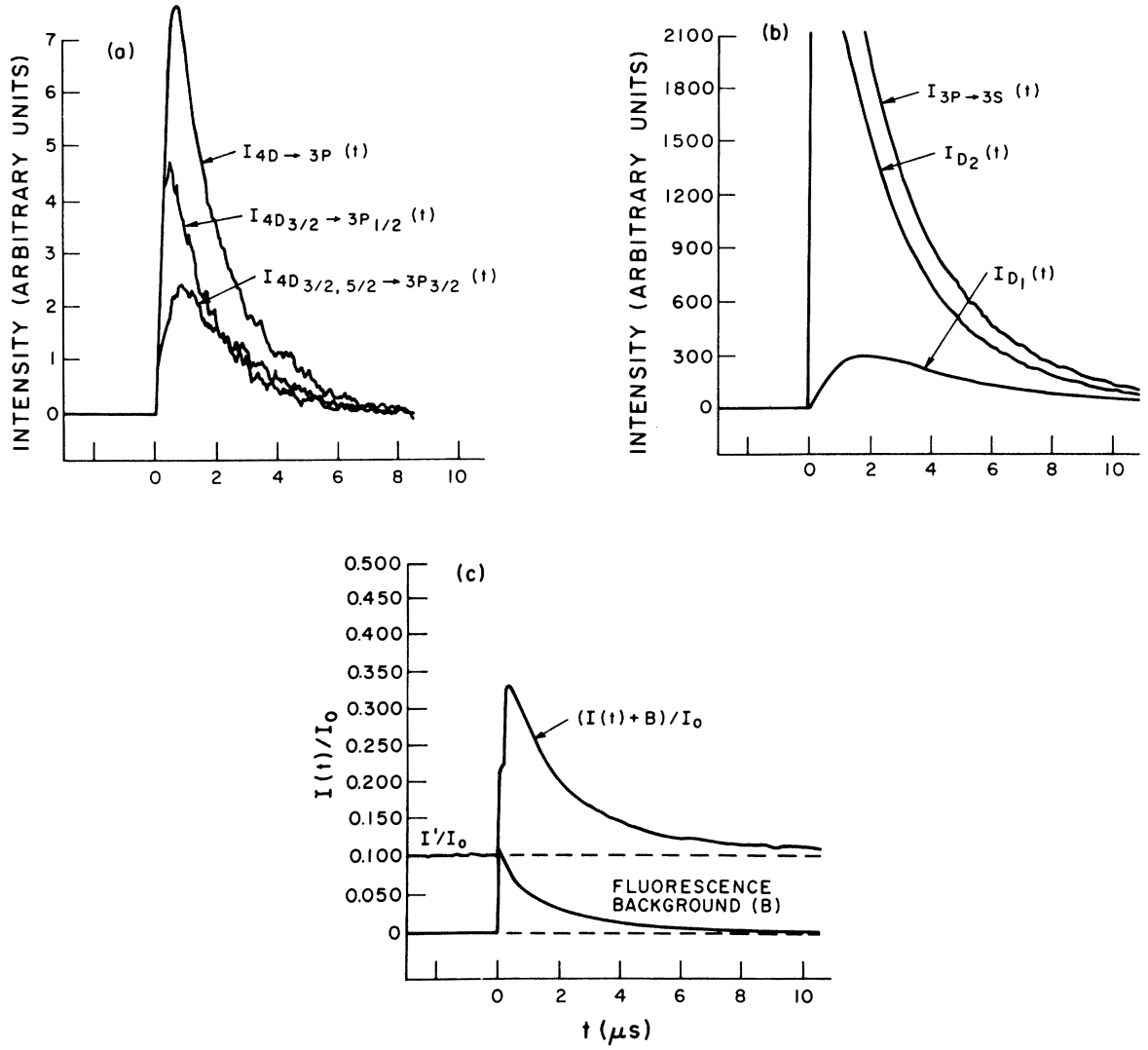

FIG. 4. (a) Total $4D \rightarrow 3P$ fluorescence intensity, in arbitrary units $I_{4D \rightarrow 3P}(t)$ and its two spectral components $I_{4D_{5/2,3/2} \rightarrow 3P_{3/2}}(t)$ and $I_{4D_{3/2} \rightarrow 3P_{1/2}}(t)$. The N_2 laser fired at $t=0$. (b) Total $3P \rightarrow 3S$ fluorescence signal $I_{3P}(t)$ and its two spectral components $I_{D_1}(t)$ and $I_{D_2}(t)$. Except for an $\sim 25\%$ difference in detection efficiency, this is in the same intensity units as Fig. 4(a). (c) cw-laser transmission signal with the cw laser detuned 2.4 GHz to the red of D_2-line centroid. I' is measured before the N_2 pulse. The zero point and N_2-laser induced fluorescence background were obtained by blocking the cw laser. I_0 was obtained by tuning the cw laser far from resonance. In all cases $[\mathrm{Na}]=3.6\times 10^{13}\ \mathrm{cm}^{-3}$ and the N_2-laser intensity was $\sim 3.3\times 10^4\ \mathrm{W/cm}^2$.

Conservation of atoms requires

$$\bar{n}_0(0,t)+\bar{n}_1(0,t)+\bar{n}_2(0,t)=n\ . \tag{9}$$

Combining Eqs. (7)—(9) we obtain

$$[n_1(0,t)+\tfrac{3}{2}n_2(0,t)]/n=-\ln[I(t)/I']/\ln(I'/I_0)\ , \tag{10}$$

where we have made use of the fact that $g_2/g_0=2$. Assuming that the D_1 to D_2 fluorescence ratio is independent of y (we have measured[10] this ratio as a function of y and found it is essentially constant, as expected), we may write

$$I_{D_1}(t)/I_{D_2}(t)=\Gamma_1^e\bar{n}_1(0,t)/\Gamma_2^e\bar{n}_2(0,t)\ , \tag{11}$$

which can be combined with the fact that $\bar{n}_{3P}(0,t)=\bar{n}_1(0,t)+\bar{n}_2(0,t)$ to yield

$$\bar{n}_2(0,t)=\bar{n}_{3P}(0,t)I_{D_2}(t)\Gamma_1^e/[I_{D_1}(t)\Gamma_2^e+I_{D_2}(t)\Gamma_1^e] . \tag{12}$$

Finally, inserting Eq. (12) into Eq. (10) yields

$$\frac{\bar{n}_{3P}(0,t)}{n}=\frac{-\ln[I(t)/I']}{\ln(I'/I_0)}\left[\frac{2[I_{D_1}(t)\Gamma_2^e+I_{D_2}(t)\Gamma_1^e]}{2I_{D_1}(t)\Gamma_2^e+3I_{D_2}(t)\Gamma_1^e}\right] . \tag{13}$$

Since $0<\bar{n}_1(0,t)<0.5\bar{n}_2(0,t)$ for laser pumping of D_2, the term in large parentheses in Eq. (13) lies between the limits $\frac{2}{3}$ and $\frac{3}{4}$. Thus although n_1/n_2 is fairly well known, the measurement of the $3P$-atom column density is very insensitive to the ratio n_1/n_2.

Measurements were made at several cw laser detunings and intensities to guarantee that the signals were not distorted by optical pumping by the cw laser. Even moderate cw intensities (~ 100 μW) at the detunings we used (>2.4 GHz) caused dramatic distortion of the cw transmission signals. The cw laser power was therefore maintained a factor of ~ 5–10 below the point where signal distortion was first observed. Within the uncertainty of these measurements (roughly 20% based on signal reproducibility), we obtained the same values for $\bar{n}_{3P}(0,t)$ independent of the cw laser frequency and power.

The excited-atom column density is obtained from these measurements of $I(t)/I_0$, I'/I_0, $I_{D_1}(t)/I_{D_2}(t)$, and an assumed ratio of Γ_1^e/Γ_2^e calculated from Holstein's[12] theory of radiation trapping in an infinite slab. The latter assumption is supported by our measured decay rates of the $3P$ fluorescence, from which we have obtained values of Γ_2^e which agree within $\sim 5\%$ uncertainty with the Holstein theory.

Figure 5 shows time-dependent excited-atom column densities as a fraction of the total sodium column density $[\bar{n}_{3P}(0,t)/n]$ for three pulsed-laser intensities. The cw laser was detuned ~ 2.4 GHz to the red of the D_2 centroid for this data. Note the apparent saturation, with increasing power, of the $3P$ population at high pulsed-laser powers. At the highest power, an extrapolation back to $t=0$ yields $\bar{n}_{3P}(0,0)>0.4n$.

Immediately following a saturating pulse that fills the entire cell, the vapor is optically thin to resonance radiation and the fluorescence decays with the rate Γ_N. Only when $n_{3S}\gg n_{3P}$ does the $3P$ population decay with the rate Γ_{3P}^e. Thus in the first few natural lifetimes after the pulse, the $3P$ density is expected to decay more rapidly than a linear extrapolation back to $t=0$ in Fig. 5 would indicate. This effect cannot be accurately evaluated from the data of Fig. 4 due to the response time of the electronics (~ 20 ns rise time). We believe, however, that the highest power data shown in Fig. 5 are consistent with an initially almost completely saturated $3P_{3/2}$ population [i.e., $n_{3P_{3/2}}(t=0)=n_{3S}$, $n_{3P_{1/2}}(t=0)=0$ would yield $n_{3P}/n=0.5$].

Once the $3P$-atom column density $\bar{n}_{3P}(0,t)$ is known, we need to obtain the $3P$-atom spatial distribution. We make the assumption that the x and y dependences of $n_{3P}(x,y,t)$ are independent of t and separable (the symmetry of the cell and excitation geometries indicate that all densities are independent of z—see Fig. 3), i.e., we take

$$n_{3P}(x,y,t)=\bar{n}_{3P}(y=0,t)\phi(x)\beta(y) . \tag{14}$$

The function $\phi(x)$ is normalized as

$$\int \phi(x)\,dx=1 ,$$

and is taken from van Trigt's[13] calculations of the fundamental-mode excited-atom spatial distribution across an infinite slab. (Van Trigt's calculations are based on Holstein's theory incorporating some minor improvements. The results, however, agree well with those obtained by Holstein.) The good agreement between our measured values[10] of Γ_2^e and Holstein's infinite slab calculations indicate that this is a good approximation for $\phi(x)$. $\beta(y)$ is taken

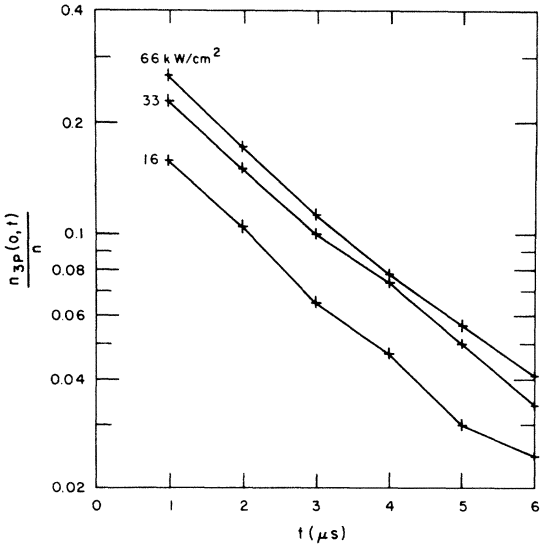

FIG. 5. Excited-atom density (as a fraction of the total Na density) vs time after the laser pulse for three laser intensities 6.6×10^4, 3.3×10^4, and 1.6×10^4 W/cm^2. [Na]$=3.6\times10^{13}$ cm^{-3}. Pulsed-laser frequency was that of the D_2 line.

from measurements we made of the $3P$ fluorescence as a function of y across the window face (see Ref. 10). From Eq. (14) and the definition of $\bar{n}_{3P}(y,t)$ it follows that $\beta(0)=1$ and $\beta(y)$ is therefore not normalized, i.e.,

$$\int \beta(y)\,dy \equiv \bar{\beta}(y) .$$

IV. RATE EQUATION MODEL FOR THE ENERGY-TRANSFER PROCESS

After the brief (~ 5 ns) excitation of the $3P$ level, the following rate equations apply:

$$\begin{aligned}\dot{n}_{3P} &= -\Gamma^e_{3P} n_{3P} - n^2_{3P}(k_{4D}+k_{5S}+k_{4F}+k_{\mathrm{AI}}) \\ &\quad + \sum_{JJ'} \Gamma^e_{4D_J\to 3P_{J'}} n_{4D_J} + \sum_{J'} \Gamma^e_{5S\to 3P_{J'}} n_{5S} ,\end{aligned} \tag{15}$$

$$\begin{aligned}\dot{n}_{4D_J} &= -\sum_{J'} (\Gamma^e_{4D_J\to 3P_{J'}} + \Gamma_{4D_J\to 4P}) n_{4D_J} \\ &\quad + k_{4D} n^2_{3P} \frac{g_J}{10} \\ &\equiv -\Gamma^e_{4D_J} n_{4D_J} + k_{4D} n^2_{3P} \frac{g_J}{10} .\end{aligned} \tag{16}$$

Here $J=\frac{5}{2}, \frac{3}{2}$ and $J'=\frac{3}{2}, \frac{1}{2}$ and we have assumed that since the $4D$ fine-structure levels are essentially degenerate, they are produced in their statistical ratio $g_J/10$. We also neglect $4D_J \leftrightarrow 4D_{J'}$ mixing since it is slow compared to $\Gamma^e_{4D_J}$.

In Eqs. (15) and (16) k_{4D}, k_{5S}, and k_{4F} are rate coefficients for producing $4D$, $5S$, and $4F$, respectively, and k_{AI} is the associative ionization $[\mathrm{Na}(3P)+\mathrm{Na}(3P)\to \mathrm{Na}_2^+ + e^-]$ rate coefficient (see Fig. 1). An equation equivalent to Eq. (16) applies to the $5s$ level. Radiative transitions to the $4P$ level are optically thin but radiation emitted in transitions to the $3P$ level may be trapped and are represented by effective rates Γ^e. For our sodium densities, processes such as excitation transfer to other levels, the reverse process to Eq. (1), quenching collisions, etc., are not significant compared to the above radiative rates.

The second to fourth terms on the right-hand side of Eq. (15) are much smaller than the first, radiative-decay term. Furthermore, we observe a very nearly exponential decay of n_{3P} in the late time, so that these minor corrections can be included in the observed Γ^e_{3P}. Equation (15) thus reduces to a simple equation with the solution

$$n_{3P}(t) = n_{3P}(0)\exp(-\Gamma^e_{3P} t) . \tag{17}$$

Inserting this into Eq. (16) yields

$$n_{4D_J}(t) = \frac{g_J}{10} \frac{k_{4D}[n_{3P}(0)]^2}{\Gamma^e_{4D_J} - 2\Gamma^e_{3P}} (e^{-2\Gamma^e_{3P} t} - e^{-\Gamma^e_{4D_J} t}) . \tag{18}$$

Since $\Gamma^e_{4D_J} \geq \Gamma_{4D\to 4P} = 6.7\times 10^{-6}$ s^{-1} (Ref. 8) and $\Gamma^e_{3P} \leq 0.27\times 10^{-6}$ s^{-1} at the densities used in this experiment, the second exponential in Eq. (18) is negligible compared to the first for $t > 10^{-6}$ s; i.e., owing to the rapid $4D$-level decay, $n_{4D_J}(t)$ depends only on $n_{3P}(t)$ and not on past history. Because of this our approximation of taking $\Gamma^e_{4D_J}$ as constant in (16) and (18) is valid. Thus

$$\begin{aligned}n_{4D_J}(t) &= \frac{g_J}{10} \frac{k_{4D}[n_{3P}(0)]^2 e^{-2\Gamma^e_{3P} t}}{\Gamma^e_{4D_J} - 2\Gamma^e_{3P}} \\ &= \frac{g_J}{10} \frac{k_{4D}[n_{3P}(t)]^2}{\Gamma^e_{4D_J} - 2\Gamma^e_{3P}} .\end{aligned} \tag{19}$$

Equation (19) predicts that n_{4D} decays with the rate $2\Gamma^e_{3P}$, which was in fact observed [see Figs. 4(a) and 4(b)].

Equations (17) and (19) apply to one position (x,y,z) in the cell, so that a volume integral is needed to describe the total populations. Furthermore, the measured intensities depend on radiative escape probabilities, which are also position dependent. To obtain the measured $4D\to 3P$ to $3P\to 3S$ fluorescence ratio, we consider the cell geometry depicted in Fig. 3. The $4D_J\to 3P_{J'}$ fluorescence emitted at time t from the volume element $dx\,dy\,dz$ at x,y,z is

$$\hbar\omega_{4D\to 3P} n_{4D_J}(x,y,t)\Gamma_{4D_J\to 3P_{J'}}\,dx\,dy\,dz ,$$

where we have noted that the population is independent of z due to the symmetry of the cell and excitation source. The probability that such a fluorescence photon is emitted into the detection solid angle $d\Omega$ and traverses the distance x without being absorbed is

$$P_{4D_J\to 3P_{J'}}(x,y,t)(d\Omega/4\pi) ,$$

where we note that since the $3P$ atoms are unpolarized due to radiation trapping, the $4D$ fluorescence emission should also be unpolarized and isotropic. Thus the detected $4D\to 3P$ fluorescence signal from this volume element is

$$I_{4D\to 3P}(x,y,z,t)\,dx\,dy\,dz = \frac{d\Omega}{4\pi} \hbar\omega_{4D\to 3P} \sum_{JJ'} n_{4D_J}(x,y,t)\Gamma_{4D_J\to 3P_{J'}} P_{4D_J\to 3P_{J'}}(x,y,t)\,dx\,dy\,dz , \tag{20}$$

where J is $\frac{5}{2}$ or $\frac{3}{2}$ and J' is $\frac{3}{2}$ or $\frac{1}{2}$. Similarly, the detected $3P\rightarrow 3S$ fluorescence signal from this volume element is

$$I_{3P\rightarrow 3S}(x,y,z,t)\,dx\,dy\,dz=\frac{d\Omega}{4\pi}\hbar\omega_{3P\rightarrow 3S}\sum_{J'}n_{3P_{J'}}(x,y,t)\Gamma_{3P_{J'}\rightarrow 3S}P_{3P_{J'}\rightarrow 3S}(x,y,t)\,dx\,dy\,dz\ . \tag{21}$$

The total fluorescence signals $I_{4D\rightarrow 3P}(t)$ and $I_{3P\rightarrow 3S}(t)$ are obtained by integrating these expressions over the detected volume.

Using Eq. (19) for $n_{4D_J}(t)$ in Eq. (20) and noting that $\Gamma_{3P_{J'}\rightarrow 3S}$ is independent of J', we obtain

$$\frac{I_{4D\rightarrow 3P}(t)}{I_{3P\rightarrow 3S}(t)}=\frac{k_{4D}\omega_{4D\rightarrow 3P}}{\Gamma_{3P\rightarrow 3S}\omega_{3P\rightarrow 3S}}\times\int\int dx\,dy[n_{3P}(x,y,t)]^2\times\sum_{JJ'}\left[\frac{g_J}{10}\frac{\Gamma_{4D_J\rightarrow 3P_{J'}}}{\Gamma^e_{4D_J}-2\Gamma^e_{3P}}P_{4D_J\rightarrow 3P_{J'}}(x,y,t)\right]\Big/\int\int dx\,dy\sum_{J'}n_{3P_{J'}}(x,y,t)P_{3P_{J'}\rightarrow 3S}(x,y,t)\ . \tag{22}$$

Equation (22) can be inverted to yield the rate coefficient k_{4D}:

$$k_{4D}=\frac{I_{4D\rightarrow 3P}(t)\omega_{3P\rightarrow 3S}\Gamma_{3P\rightarrow 3S}\bar{\beta}(y)\bar{n}_{3P}(0,t)(\Gamma_{4D\ \mathrm{nat}}-2\Gamma^e_{3P})T_{3P}(t)}{I_{3P\rightarrow 3S}(t)\omega_{4D\rightarrow 3P}[\bar{n}_{3P}(0,t)]^2\Gamma_{4D\rightarrow 3P}\int[\phi(x)]^2dx\int[\beta(y)]^2dyT_{4D}(t)} \tag{23}$$

with

$$T_{3P}(t)=\int\int dx'\,dy'\left[\phi(x')\beta(y')\left[\frac{\bar{n}_1(t)}{\bar{n}_{3P}(t)}P_{3P_{1/2}\rightarrow 3S}(x',t)+\frac{\bar{n}_2(t)}{\bar{n}_{3P}(t)}P_{3P_{3/2}\rightarrow 3S}(x',t)\right]/\bar{\beta}(y)\right] \tag{24}$$

and

$$\begin{aligned}T_{4D}(t)=\int\int dx'\,dy'([\phi(x')\beta(y')]^2[0.6\Gamma_{4D_{5/2}\rightarrow 3P_{3/2}}P_{4D_{5/2}\rightarrow 3P_{3/2}}(x',y',t)/(\Gamma^e_{4D_{5/2}}-2\Gamma^e_{3P})]\\+\{0.4[\Gamma_{4D_{3/2}\rightarrow 3P_{3/2}}P_{4D_{3/2}\rightarrow 3P_{3/2}}(x',y',t)\\+\Gamma_{4D_{3/2}\rightarrow 3P_{1/2}}P_{4D_{3/2}\rightarrow 3P_{1/2}}(x',y',t)]/(\Gamma^e_{4D_{3/2}}-2\Gamma^e_{3P})\})\\\times(\Gamma_{4D\ \mathrm{nat}}-2\Gamma^e_{3P})/\left[\Gamma_{4D\rightarrow 3P}\int[\beta(y)]^2dy\int[\phi(x)]^2dx\right],\end{aligned} \tag{25}$$

where we have used Eq. (14) for $n_{3P}(t)$ and where the factors $\bar{\beta}(y)$, $\Gamma_{4D\rightarrow 3P}$, $\int[\beta(y)]^2dy$, $\int[\phi(x)]^2dx$, and $(\Gamma_{4D\ \mathrm{nat}}-2\Gamma^e_{3P})$ have been introduced so that the quantities T_{3P} and T_{4D} reduce to 1 in the absence of trapping and are therefore useful in estimating the magnitude of these effects. Here

$$\Gamma_{4D\ \mathrm{nat}}\equiv\Gamma_{4D\rightarrow 3P}+\Gamma_{4D\rightarrow 4P}\ .$$

We note that the measured $\beta(y)$ lead to $\int\beta(y)\,dy=0.82$ to 0.86 and $\int[\beta(y)]^2dy=0.70$ to 0.75 for the Na densities studied; this ratio of 0.70/0.82 or 0.75/0.86 represents essentially the correction due to the nonuniform distribution of n_{3P} in the y direction, which enters the energy-transfer process in $I_{4D\rightarrow 3P}$ as $\int[n_{3P}(y)]^2dy$ and in $I_{3P\rightarrow 3S}$ as $\int n_{3P}(y)\,dy$. For the same reason, the distribution of n_{3P} in the x direction, using the slab fundamental-mode distribution,[13] leads to a correction $\int[\phi(x)]^2dx=1.09$ to 1.13.

Equation (23) represents a corrected version of Eq. (4), with the differences being the inclusion of the differential trapping of the various fine-structure components and the spatial dependence of the excited-atom density and of the trapping. Owing to the fact that the $4D\rightarrow 3P$ trapping averaged over fine-structure components is not too severe at the times we are observing (see values of T_{4D} in Table I), and that the excited-atom spatial distributions do not vary rapidly over the detected volume, the results obtained from Eq. (4), ignoring all of these effects including all $4D\rightarrow 3P$ trapping, agree with those from Eq. (23) to within approximately a factor of 2.

V. RESULTS

Measurements of $I_{4D\rightarrow 3P}(t)/I_{3P\rightarrow 3S}(t)$, $I_{D_1}(t)/I_{D_2}(t)$, $n_{3P}(0,t)$, and the distribution of excit-

TABLE I. Determination of rate coefficients k_{4D} and k_{5S}.

[Na] (10^{13} cm^{-3})	Laser intensity (kW/cm^2)	t (μs)	$\bar{n}_{3P}(0,t)$[a] (10^{12} cm^{-3})	$T_{3P}(t)$[b]	$T_{4D}(t)$[c]	$T_{5S}(t)$[d]	$\frac{I_{4D\to 3P}(t)}{I_{3P\to 3S}(t)}$	$\frac{I_{5S\to 3P}(t)}{I_{3P\to 3S}(t)}$	k_{4D}[e] (10^{-10} cm^3/s)	k_{5S}[f] (10^{-10} cm^3/s)
9.09	66	3	15.0	0.003 02	0.710		4.07×10^{-3}		1.12	
9.09	33	3	11.0	0.003 02	0.749		4.28×10^{-3}		1.53	
9.09	16	3	5.2	0.003 02	0.860		3.07×10^{-3}		2.02	
9.09	66	5	8.3	0.003 04	0.796	0.954	3.30×10^{-3}	3.67×10^{-3}	1.48	1.69
9.09	33	5	6.6	0.003 04	0.831	0.964	3.47×10^{-3}	3.18×10^{-3}	1.87	1.83
9.09	16	5	3.4	0.003 04	0.913	0.983	2.15×10^{-3}	1.54×10^{-3}	2.05	1.68
3.58	66	4	2.6	0.007 22	0.929	0.978	8.81×10^{-4}	5.99×10^{-4}	2.40	1.90
3.58	33	4	2.3	0.007 22	0.939	0.980	7.98×10^{-4}	4.31×10^{-4}	2.43	1.54
3.58	16	4	1.6	0.007 22	0.960	0.984	5.95×10^{-4}	2.24×10^{-4}	2.55	1.15

[a]Excited-atom density from Eq. (13).
[b]Effects of $3P\to3S$ fluorescence trapping from Eq. (24).
[c]Effects of $4D\to3P$ fluorescence trapping from Eq. (25).
[d]Effects of $5S\to3P$ fluorescence trapping from Eq. (28).
[e]k_{4D} from Eq. (23).
[f]k_{5S} from Eq. (23) with $4D$ replaced by $5S$.
Note: $\Gamma_{3P\to3S}=6.30\times10^7$ s^{-1}, $\Gamma_{4D_{5/2}\to3P_{3/2}}=1.31\times10^7$ s^{-1}, $\Gamma_{4D_{3/2}\to3P_{3/2}}=2.19\times10^6$ s^{-1}, $\Gamma_{4D_{3/2}\to3P_{1/2}}=1.09\times10^7$ s^{-1},
$\Gamma_{4D\to4P}=6.7\times10^6$ s^{-1}, $\Gamma_{5S\to3P_{3/2}}=4.82\times10^6$ s^{-1}, $\Gamma_{5S\to3P_{1/2}}=2.41\times10^6$ s^{-1} (from Ref. 8).
$\Gamma_{5S\to4P}=5.4\times10^6$ s^{-1} (from Ref. 14).

ed atoms in the y direction $\beta(y)$ were made at two sodium densities (9.1×10^{13} and 3.6×10^{13} cm^{-3}) and with three different pulsed-laser intensities. In all cases, the pulsed-laser frequency at the D_2 line was set by maximizing the D_1 sensitized fluorescence signal. The escape probabilities P are calculated as outlined in the Appendix. $\Gamma^e_{3P_{3/2}}$ was measured from the late-time fluorescence decay rate and the ratio $\Gamma^e_{3P_{1/2}}/\Gamma^e_{3P_{3/2}}$ was taken from Holstein's theory.[12]

The various $\Gamma^e_{4D_J\rightarrow3P_{J'}}$ were calculated as described in Ref. 10 using approximations that are valid at relatively low optical depths. In particular we used a single effective absorption coefficient for the entire line and assumed that since the optical depths are not very large and $n_{4D}\propto(n_{3P})^2$, n_{4D} is concentrated near the laser axis and we could assume all $4D$ atoms are effectively at the cell center ($x=L/2$). Additionally, we assumed that since n_{4D} is small at y values outside the detected zone (see Fig. 3), $4D\rightarrow3P$ fluorescence photons emitted outside the detected zone are seldom trapped inside the zone; thus we consider an escape as occurring whenever a 569-nm photon leaves the detected zone. Minor errors due to these last two assumptions tend to cancel. The escape factors determined in this way

$$(g\equiv\Gamma^e_{4D_J\rightarrow3P_{J'}}/\Gamma_{4D_J\rightarrow3P_{J'}})$$

lie between ~0.2 and 1. For $g\sim1$ we have $\Gamma^e_{4D_J}\sim\Gamma_{4D_J\,\mathrm{nat}}$, and little uncertainty is introduced into $\Gamma^e_{4D_J}$ by uncertainty in the escape factors. Similarly for $g\ll1$ we find $\Gamma^e_{4D_J}\sim\Gamma_{4D_J\rightarrow4P}$, and little uncertainty results. Near $g\sim0.5$ we estimate that the $\Gamma^e_{4D_J\rightarrow3P_{J'}}$ are accurate to at least $\pm30\%$, which introduces uncertainties into $\Gamma^e_{4D_J}$ of not more than $\sim\pm15\%$.

Natural radiative-decay rates were taken from Refs. 8 and 14; the values used are given in Table I. The detection system efficiency factors ϵ_i, used to convert photomultiplier currents to intensities, were measured at the detected wavelengths of 569, 616, and 589 nm with a calibrated tungsten iodide lamp. Here the important parameter is the lamp emission per unit wavelength, since the spectrometer dispersion (Å/mm) is constant to within 1% over the relevant frequency interval. We obtain $\epsilon_{3P}/\epsilon_{4D}=0.753$ and $\epsilon_{3P}/\epsilon_{5S}=1.506$. The difference between these numbers is due to the photomultiplier cathode response and the spectrometer grating efficiency. Finally, the integrals in T_{4D} and T_{3P} were carried out numerically. Details of the calculations can be found in Ref. 10. [Note, however, a slight difference between the present definition of T_{4D} and T_{5S} and the definitions of Q_{4D} and Q_{5S} in Ref. 10, which corrects a minor error in Ref. 10. Other minor errors in Ref. 10 such as an incorrect value of $\Gamma_{5S\rightarrow4P}$ and failure to include the term $\omega_{3P\rightarrow3S}/\omega_{4D\rightarrow3P}$ in the expression for k_{4D} have also been corrected here. The present results also supercede those we presented at the August 1982 International Conference on Atomic Physics (ICAP) which were subject to some of the same errors.] The results are tabulated in Table I.

At higher density, and especially at the highest power, we obtain a result for k_{4D} which is not in good agreement with our low-density results (see Table I). The causes for this systematic effect are not well understood, but the power-dependent terms in Eq. (23) (T_{4D} and $\Gamma^e_{4D\rightarrow3P}$) do not vary sufficiently to explain it. Other possible explanations of this effect will be explored in the next section. For reasons given there, we use the average of the three lower density measurements for the $4D$ energy pooling rate coefficient

$$k_{4D}=2.46\times10^{-10}\ \mathrm{cm}^3/\mathrm{s}\pm35\% \ . \tag{26}$$

A similar analysis has been carried out on the $5S$ level. Equation (23) remains valid if we replace $4D$ by $5S$ everywhere. We must, however, use

$$\Gamma^e_{5S}\equiv\Gamma_{5S\rightarrow4P}+\Gamma^e_{5S\rightarrow3P_{1/2}}+\Gamma^e_{5S\rightarrow3P_{3/2}} \tag{27}$$

and

$$T_{5S}(t)=\int\int dx'\,dy'\left\{[\beta(y')\phi(x')]^2[\Gamma_{5S\rightarrow3P_{3/2}}P_{5S\rightarrow3P_{3/2}}(x',y',t)+\Gamma_{5S\rightarrow3P_{1/2}}P_{5S\rightarrow3P_{1/2}}(x',y',t)]\right.$$
$$\left.\times(\Gamma_{5S\,\mathrm{nat}}-2\Gamma^e_{3P})/\{(\Gamma^e_{5S}-2\Gamma^e_{3P})\Gamma_{5S\rightarrow3P}\int[\beta(y)]^2dy\int[\phi(x)]^2dx\}\right\} . \tag{28}$$

The $5S$ results are also listed in Table I. We obtain

$$k_{5S}=1.63\times10^{-10}\ \mathrm{cm}^3/\mathrm{s}\pm35\% \ , \tag{29}$$

where we have averaged all measurements at both densities since no systematic effects at high power and high density were observed in this case. The average cross sections σ_{nL} are obtained from

$$\sigma_{nL}\equiv k_{nL}/\bar{v} \ , \tag{30}$$

where $\bar{v}$ is the mean interatomic velocity [$\bar{v}=(8kT/\mu\pi)^{1/2}$]. We then obtain

$$\sigma_{4D}=2.3\times10^{-15}\ \mathrm{cm}^2\pm35\% \tag{31}$$

and

$$\sigma_{5S}=1.6\times10^{-15}\ \text{cm}^2\pm35\% \ . \tag{32}$$

We also observed very weak signals from the $6S$ and $5D$ levels. These were, in fact, too weak to obtain quantitative values of σ_{6S} and σ_{5D} except at the highest density and power where the temporal behavior indicates these levels are primarily populated not by Na($3P$)-Na($3P$) collisions, but rather through recombination. Nevertheless, we can give an upper limit to σ_{6S} and σ_{5D} of 6×10^{-17} and 1×10^{-16} cm^2, respectively.

The estimated uncertainties appearing in the rate coefficients in Eqs. (26) and (29) were determined as follows. The ratio of $4D\rightarrow3P$ (or $5S\rightarrow3P$) fluorescence to $3P\rightarrow3S$ fluorescence is probably uncertain by $\sim15\%$ owing to uncertainties in timing, transient digitizer nonlinearities, shot-to-shot power and frequency variations in the pulsed-laser output, and the uniformity and accuracy of calibration of the neutral density filters which were used. Averaging, as we did, over 64 shots, typically reduces the statistical uncertainty to less than 5%. Calculation of the $3P\rightarrow3S$ escape probability in the detection direction is probably accurate to 5% at these densities (based on comparisons of the measured Γ^e_{3P}'s with those calculated using Holstein's theory in an infinite slab geometry), while the $4D\rightarrow3P$ and $5S\rightarrow3P$ escape probabilities may be uncertain by as much as 10% owing primarily to the use of an effective absorption coefficient. The measurement of $\bar{n}_{3P}(0,t)$ is subject to most of the same uncertainties as the fluorescence ratio, but it is also influenced by cw-laser frequency drifts and slight problems with the photomultiplier gating system. Additionally, as one transient digitizer was used alternately for averaging all signals, the measurements of $\bar{n}_{3P}(0,t)$ and $I_{4D\rightarrow3P}(t)/I_{3P\rightarrow3S}(t)$ were not made simultaneously, and therefore experimental drifts were more important. The laser parameters were, however, stable to within a few percent over the time scale of interest and the sodium density was stable to a couple percent and known to at least 10%. We therefore assign an uncertainty of $\sim20\%$ to the values of $\bar{n}_{3P}(0,t)$. The detection system efficiencies were measured to $\sim5\%$ subject primarily to the accuracy of the calibration of the lamp spectral profile. As stated earlier, $\Gamma^e_{4D_J}$ and Γ^e_{5S} were uncertain by not more than $\sim15\%$. Finally, we estimate that the calculated function $\phi(x)$ and measured function $\beta(y)$ contribute uncertainties of not more than 10% to the rate coefficients.

Assuming there are no correlations among the systematic errors, we can combine the various uncertainties in quadrature and arrive at the overall uncertainties listed in Eqs. (26) and (29). We believe these uncertainties are fairly conservative.

VI. DISCUSSION

The measured values of k_{4D}, listed in Table I, are seen to decrease with increasing power at the higher Na density. There are several mechanisms which may be contributing to this change. First, we have noted that at high densities and high powers, self-focusing is occurring. This will enhance the local power density, so that ionization can occur. The abrupt onset of this hypothesized ionization implies a nonlinear laser intensity dependence which favors multiphoton ionization occurring in the regions where the power is enhanced. (Collisional ionization mechanisms should not show this intensity dependence since the $3P$ population is nearly saturated in our experiment.) The resulting electrons, which diffuse to the walls at the ambipolar diffusion rate, undergo quenching collisions with Na($3P$) atoms and increase the observed $3P$ decay rate throughout the measured time interval. This electron quenching of $3P$ atoms does not cause any error in Eq. (23) since the actual $3P$ density at time t was measured and used to obtain k_{4D} (and owing to the rapid decay of $4D$, the $4D$ population at t only depends on the $3P$ population at t). However, these electrons also undergo inelastic collisions with $4D$ atoms. The only process that might be fast enough to depopulate $4D$ at a rate comparable to the radiative rate Γ^e_{4D} is $4D\rightarrow4F$ transfer where $\Delta E\sim40$ cm^{-1} (see Fig. 1). The fact that k_{5S} does not show a similar drop at high density and high power (Table I) is consistent with this model as $5S$ lies much further from other sodium levels. Order-of-magnitude estimates indicate that the number of electrons produced by multiphoton ionization in enhanced intensity regions is sufficient to produce a $4D\rightarrow4F$ transfer rate that competes significantly with Γ^e_{4D}.

At the lower Na density this increase in the $3P$-atom decay rate is not observed, and self-focusing effects are also greatly diminished. Thus we believe our low-density measurements of k_{4D} are accurate within the stated uncertainties (see Sec. V), as is the low-power, high-density measurement.

In addition to the above measurements of time-dependent fluorescence following pulsed excitation, we have measured the ratio of the $4D\rightarrow3P$ to $5S\rightarrow3P$ fluorescence using low-power cw excitation for $T=538$–735 K. In this case, the excited-atom population is small and no trapping of upper-level fluorescence is expected. From Eq. (4) we expect for these conditions

$$\frac{k_{4D}}{k_{5S}}=\frac{I_{4D\rightarrow3P}}{I_{5S\rightarrow3P}}\frac{\Gamma_{4D}}{\Gamma_{4D\rightarrow3P}}\frac{\Gamma_{5S\rightarrow3P}}{\Gamma_{5S}}\frac{\omega_{5S\rightarrow3P}}{\omega_{4D\rightarrow3P}} \ . \tag{33}$$

Results obtained from Eq. (33) and the measured

fluorescence ratio, which will be presented elsewhere, are consistent with our pulsed results and with a k_{5S} independent of T and an $\exp(-\Delta E_{4D}/kT)$ temperature dependence for k_{4D}.

Table II compares our measured values of the energy pooling cross sections with those of other experiments and with theory. The preliminary values by Allegrini *et al.*[15] were reported at the August 1982 ICAP, since submission of this manuscript. Their measurements were made at relatively low optical depth and ~480 K using cw excitation. As can be seen in Table II, these σ values are of the same order of magnitude as ours.

As can also be seen in Table II, our results are a factor of ~300 greater than those measured by Krebs and Schearer[7] and more than 10^4 times larger than those measured by Kushawaha and Leventhal.[6] We will now consider possible explanations of these enormous discrepancies.

The experiment of Kushawaha and Leventhal was carried out using a cw laser. Because of this, it was not possible to obtain fluorescence decay rates and therefore to accurately include effects of radiation trapping. In particular, no account of trapping of upper-level fluorescence was made. Additionally, the $3P$ density was not measured, but was assumed to be saturated. The fluorescence versus intensity data presented in Ref. 6 are certainly less than convincing on this point although the intensity where they first observe "saturation" (~10 W/cm^2) is not too far from the single-atom saturation intensity.[10] On the other hand, this intensity is at least five orders of magnitude greater than is necessary for optical pumping effects to become important and far below that necessary to saturate a dense column of atoms. It is possible that the $3P$ density was very much less than the assumed saturation value. However, the most crucial error of Ref. 6 is the assumption that the excited atoms were confined essentially to the region of the focused laser beam. This is certainly not the case in the presence of radiation diffusion, where the excited atoms quickly spread throughout almost the entire cell volume. Since the rate coefficients k_{nL} are proportional to $(n_{3P})^2$ (see Ref. 6), the error in k_{nL} is proportional to the fourth power of the cell diameter divided by the laser beam diameter, which can be many orders of magnitude for a tightly focused beam. Finally, we mention that Kushawaha and Leventhal did not measure a fluorescence ratio, and therefore the absolute efficiency of their detection system enters their calculations directly. This is a quantity that is often difficult to determine accurately.

The experiment of Krebs and Schearer[7] was similar in design to ours. They used a nitrogen-laser pumped dye laser excitation and time resolved both the $4D \rightarrow 3P$ and $3P \rightarrow 3S$ fluorescence signals. However, most of the objections that appeared in the

TABLE II. Comparison of experimental and theoretical determinations of the $4D$ and $5S$ energy pooling cross sections.

Source	σ_{4D} (cm^2)	σ_{5S} (cm^2)	$\frac{\sigma_{4D}}{\sigma_{5S}}$	T(K)
Experiment				
This work	$2.3\times10^{-15}\pm35\%$	$1.6\times10^{-15}\pm35\%$	1.51	~597
			1.73	652
Kushawaha and Leventhal (Ref. 6)	4.5×10^{-20}	7.3×10^{-20}	0.62	~487
Krebs and Schearer (Ref. 7)	9.0×10^{-18}			670
Allegrini *et al.* (Ref. 15)	1.9×10^{-15}	7.8×10^{-16}	2.4	483
Allegrini *et al.* (Ref. 1)			1	593
			0.7	553
			0.4	523
Theory				
Kowalczyk (Ref. 17)	$>2.3\times10^{-16}$			550
	$>3.9\times10^{-16}$			600
	$>6.1\times10^{-16}$			650
	$>8.6\times10^{-16}$			700

discussion of Ref. 6 also apply here. In particular, Krebs and Schearer also assumed that the excited atoms were confined to the focused laser column.[16] Again, this can lead to errors of many orders of magnitude. Additionally, trapping of $4D \rightarrow 3P$ fluorescence was not taken into account, and they assumed a saturated $3P$ population. Finally, we note that Krebs and Schearer worked at densities much higher than those where we begin to see a drop in k_{4D} which we attribute to electron collisional quenching.

Also included in Table II is σ_{4D} calculated by Kowalczyk[17] for curve crossings that occur at very large internuclear separations (~ 15 Å). Since transitions at smaller separations will also contribute to the total cross section, Kowalczyk argued that this calculation should be considered a lower bound on σ_{4D}, and indeed we observed approximately six times larger cross section. We note that Kowalczyk also did not consider the contribution of ion-pair configurations. Additionally, we note that the large temperature dependence of the calculated σ_{4D}'s (see Table II) are in fact the temperature dependence of the long-range part only. We expect that calculations including all other curve crossings would not show such pronounced temperature dependence, although our experiment did not test this point.

An experiment related to ours is that of Yabuzaki *et al.*[18] in which the inverse of the energy pooling reaction was observed in cesium vapor illuminated by a laser tuned to the $6P \rightarrow 6D$ transition

$$\mathrm{Cs}(6D_{3/2}) + \mathrm{Cs}(6S_{1/2}) \rightarrow \mathrm{Cs}(6P) + \mathrm{Cs}(6P) \ . \quad (34)$$

The value of $|\Delta E/kT| \sim 1.5$ in this Cs experiment, and similar values occur in the present Na experiment. The cross section Yabuzaki *et al.* obtained for this process (34) was 1.5×10^{-14} cm^2, which is in qualitative agreement with what we observe for the inverse process in Na. Borodin and Komarov[19] have calculated the cross section for the inverse of process (34) to be 1.5×10^{-14} cm$^2 < \sigma < 2.0 \times 10^{14}$ cm^2, while Klyucharev and Lazarenko[20] have experimentally put an upper bound of $\sigma < 10^{-13}$ cm^2 for the inverse of process (34).

Finally, we note that the gas kinetic cross section is roughly 10^{-14} cm^2 for collisions between two Na($3P$) atoms, so that σ_{4D} and σ_{5S} are a significant fraction of this. Excitation transfer processes which occur via long-range interactions usually have cross sections which are a large fraction of gas kinetic, provided $|\Delta E|$ is not too large. (In the present case, the Na_2 states that separate to $3P$, $3P$ and $3S$, $4D$ or $3S$, $5S$ are connected by the dipole-dipole interaction.) Our measurements show that the reactions studied here are no exception.

From our measurements, we obtained upper limits on σ_{6S} and σ_{5D}. These values are listed in Table III along with values for σ_{nL}'s obtained from our absolute value of σ_{5S} and the relative intensities given in Ref. 1 at $T = 593$ K. Our measured upper limits are consistent with a simple activation energy assumption:

$$\sigma_{6S}/\sigma_{4D} \sim \exp(\Delta E_{4D-6S})/kT) \sim 10^{-2} \ ,$$
$$\sigma_{5D}/\sigma_{4D} \sim \exp(\Delta E_{4D-5D}/kT) \sim 3 \times 10^{-3} \ .$$

They are also consistent with the relative intensities reported in Ref. 1.

The conclusions of other experiments must be reevaluated in light of our energy pooling cross sections. Carré *et al.*[21] have studied collisional ionization in resonantly excited sodium vapor. They observed significant Na^+ and Na_2^+ yields, but in evaluating possible ion production mechanisms, they eliminated energy pooling processes as a major contributor based on the Kushawaha and Leventhal cross sections. In fact, both ion species may be produced by processes involving $4D$ and $5S$ atoms created in energy pooling collisions, as well as in $3P$-$3P$ associative ionization. Processes such as

$$\mathrm{Na}(4D,5S,4F) + \mathrm{Na}(3S) \rightarrow \mathrm{Na}_2^+ + \mathrm{e}^- \quad (35)$$
$$\rightarrow \mathrm{Na}^+ + \mathrm{Na}^- \ , \quad (36)$$
$$\mathrm{Na}(4D,5S,4F) + \mathrm{Na}(3P) \rightarrow \mathrm{Na}^+ + \mathrm{Na} + \mathrm{e}^- \quad (37)$$
$$\rightarrow \mathrm{Na}_2^+ + \mathrm{e}^- \ , \quad (38)$$
$$\mathrm{Na}(4D,5S,4F) + \hbar\omega \rightarrow \mathrm{Na}^+ + \mathrm{e}^- \ , \quad (39)$$

need to be considered. Carré *et al.* observed

TABLE III. Sodium energy pooling cross sections at $T \sim 597$ K.

Level	σ_{nL} (cm^2)
$4D$	2.3×10^{-15} [a]
	1.3×10^{-15} [b]
$5S$	1.6×10^{-15} [a]
$6S$	$< 6 \times 10^{-17}$ [a]
	2.3×10^{-17} [b]
$5D$	$< 1 \times 10^{-16}$ [a]
	3.8×10^{-17} [b]

[a]Present results.

[b]Values computated using the present measurement of σ_{5S} and the relative intensities at $T = 593$ K given in Ref. 1. Reference 1 also reports intensities of $3D$ and $4P$ level fluorescence. These levels are, however, primarily populated through cascade and therefore we do not report these σ_{nL}'s.

enhancement of the Na^+/Na_2^+ ratio with increasing laser intensity and demonstrated that this is not simply the result of photodissociation of Na_2^+. Since processes (37) and (39) are more strongly dependent on laser power than (35) and the $3P$-$3P$ associative ionization, this behavior might be explained by these mechanisms. Carré *et al.* introduce some rather exotic laser-induced and laser-assisted mechanisms to explain their results [such as field-modified Na($3P$)-Na($3P$) associative ionization via radiative coupling with various Na_2 levels, field-assisted Na($3S$) + Na($3P$) associative ionization with absorption of one photon, and field-assisted Na($3P$) + Na($3P$) Penning ionization with absorption of one photon]. We believe, however, that their results can be easily explained by the more obvious processes of energy pooling, photoionization, and collisional and associative ionization.

Excitation transfer reactions such as (1) may play a significant role even at the low densities of atomic beams. Weiner and Polak-Dingels[22] observed Na^+ and Na_2^+ ions in collisions between two sodium beams when the interaction region was illuminated by two lasers, one resonant and one nonresonant. They also demonstrated that Na^+ is not only formed by photodissociation of Na_2^+. However, we note that reaction (1) followed by photoionization of $5S$ and $4D$ atoms may dominate even the laser-induced Penning ionization they have suggested.

Krasinski *et al.*,[23] observed $3D \rightarrow 3P$ fluorescence following cw excitation. They attempted to distinguish between direct population of $3D$ by excitation transfer in collisions of two $3P$ atoms, and population of $3D$ by recombination or by collisions of $3P$ or $3S$ atoms with hot electrons (which can be produced in any of several ionization processes). Our results indicate, however, that population of $4D$, $5S$, and $4F$ by reaction (1), followed by radiative decay to $3D$ ($4D$ and $5S$ cascade to $3D$ via the $4P$ level) should dominate the production of $3D$ atoms.

A full explanation of our observation of a drop in k_{4D} at high densities and power, and the absence of similar behavior in k_{5S}, must await further experiments. In particular the $4F$ production versus time and laser intensity should be measured. It is interesting that Müller and Hertel[5] have observed lasing at the $5S \rightarrow 4P$ wavelength in sodium vapor ($n \sim 10^{14}$ cm^{-3}) that is resonantly excited by a flash-lamp pumped dye laser (pulse duration ~ 1 μsec) in the time period before runaway ionization takes over. However, they obtain no lasing in the $4D \rightarrow 4P$ transition with their system. This result may be explained by our measured σ_{5S}/σ_{4D} ratio combined with the dependence of gain coefficients upon statistical weights and branching ratios, while the proposed $4D \rightarrow 4F$ mixing at our higher densities would further lower the $4D$ gain coefficient. (The observed decrease in k_{4D} indicates that $k_{4F}/k_{4D} < g_{4F}/g_{4D}$.)

ACKNOWLEDGMENTS

We would like to thank Dr. A. V. Phelps for many valuable discussions. This work was supported in part by National Science Foundation Grant No. PHY79-04928 through the University of Colorado.

APPENDIX: CALCULATION OF THE ESCAPE PROBABILITIES

The escape probabilities $P_{3P_{J'} \rightarrow 3S}$ depend upon the ground-state atom density, which we take to be constant throughout the cell since we are considering late times when the excited-atom density is only a few percent of the total sodium density. For the high optical depths present in our experiment, Holstein's[12] expressions for the escape probabilities are valid for all but the last few optical depths near the window:

$$P_{3P_{J'} \rightarrow 3S}(x) = [k_0(J')x]^{-1}\{\pi \ln[k_0(J')x]\}^{-1/2} \tag{A1}$$

in the density region ([Na] $\lesssim 5 \times 10^{13}$ cm^{-3}), where the radiation trapping is dominated by Doppler broadening [here $k_0(J')$ is the $3P_{J'} \rightarrow 3S$ peak absorption coefficient], and

$$P_{3P_{J'} \rightarrow 3S}(x) = [k_P(J')\pi x]^{-1/2} \tag{A2}$$

in the region ([Na] $\gtrsim 2 \times 10^{14}$ cm^{-3}), where the trapping is dominated by impact broadening. In Eq. (A2), $k_P(J')$ is given by

$$k_P(J') = \frac{\lambda^2}{2\pi} n \frac{g_2}{g_1} \frac{\Gamma_{3P_{J'} \rightarrow 3S}}{\Gamma_{\rm br}(J')} \tag{A3}$$

with $\Gamma_{\rm br}(J')$ equal to the $3P_{J'} \rightarrow 3S$ self-broadening rate. Calculations of Γ^e_{3P} using (A1), (A2), and (A3) and our measured values[10] of $\Gamma_{{\rm br}_{J'}}$ agree with our late-time measurements of the effective radiative-decay rates to within $\sim 5\%$. This level of agreement is still found even if (A2) is used at densities as low as [Na] $= 6 \times 10^{13}$ cm^{-3}. We estimate that the uncertainties in $P_{3P_{J'} \rightarrow 3S}(x)$ are $\sim 5\%$, where (A1) is used at [Na] $= 3.6 \times 10^{13}$ cm^{-3} and (A2) at [Na] $= 9.1 \times 10^{13}$ cm^{-3}.

The $4D_J \rightarrow 3P_{J'}$ escape probabilities are more complicated since this trapping depends on $n_{3P_{J'}}$ which is a function of x, y, and t. Additionally, the high optical-depth expressions (A1) and (A2) are not

valid for the relatively small n_{3P} present at the times of interest. In general, the probability $\epsilon(x,\nu)_{J'}$ of a photon of frequency ν escaping through the distance x of vapor with absorber column density

$$\bar{n}_{J'}(x,y,t) \equiv \int_0^x n_{3P_{J'}}(x',y,t)\,dx'$$

is

$$\epsilon(x,\nu)_{J'} = \exp\left[\left[-\frac{k_\nu}{n}\right]_{4D_J\rightarrow 3P_{J'}} \bar{n}_{J'}(x,y,t)\right], \tag{A4}$$

while the probability of emission $S(\nu)$ of a photon of frequency ν is $k_\nu / \int k_\nu\,d\nu$. The escape probability is obtained by integrating the product of these two probabilities over ν. A much simpler expression can be obtained by replacing k_ν with an effective absorption coefficient $\bar{k}$. This procedure was used by Milne[24] and was shown[25] to yield calculated Γ^e's which agreed with measured Γ^e's to within 10% for the sodium resonance lines at optical depths $k_0 l < 10$. We therefore expect the same procedure to be valid in the present $4D \rightarrow 3P$ case since $k_0 l < 10$ and the same Doppler broadening mechanism dominates the trapping. A reasonable choice for $\bar{k}$ is obtained from Samson's equivalent opacity (see Refs. 10 and 26). In practice we find $\bar{k}/k_0$ lies between 0.4 and 0.71.

Use of $\bar{k}$ allows $P_{4D_J\rightarrow 3P_{J'}}(x,y,t)$ to be expressed as

$$P_{4D_J\rightarrow 3P_{J'}}(x,y,t) = \exp\left[\left[-\frac{\bar{k}}{n}\right]_{4D_J\rightarrow 3P_{J'}} \bar{n}_{J'}(x,y,t)\right]. \tag{A5}$$

---

*Quantum Physics Division, National Bureau of Standards.

[1]M. Allegrini, G. Alzetta, K. Kopystynska, L. Moi, and G. Orriols, Opt. Commun. 19, 96 (1976).

[2]T. B. Lucatorto and T. J. McIlrath, Phys. Rev. Lett. 37, 428 (1976).

[3]R. M. Measures, J. Appl. Phys. 48, 2673 (1977).

[4]G. A. Victor and G. Lafyatis (private communication).

[5]W. Müller and I. V. Hertel, Appl. Phys. 24, 33 (1981); W. Müller, J. J. McClelland, and I. V. Hertel (unpublished).

[6]V. S. Kushawaha and J. J. Leventhal, Phys. Rev. A 22, 2468 (1980); 25, 570 (1982).

[7]D. J. Krebs and L. D. Schearer, J. Chem. Phys. 75, 3340 (1981).

[8]W. L. Wiese, M. W. Smith, and B. M. Miles, *Atomic Transition Probabilities,* National Bureau of Standards, National Standard Reference Data Series, No. 22, (U.S. GPO, Washington, D.C., 1969), Vol. II.

[9]J. N. Bardsley, B. R. Junker, and D. W. Norcross, Chem. Phys. Lett. 37, 502 (1976).

[10]J. P. Huennekens, Ph.D. thesis, University of Colorado, 1982 (unpublished).

[11]A. N. Nesmeyanov, *Vapor Pressure of the Elements* (Academic, New York, 1963).

[12]T. Holstein, Phys. Rev. 72, 1212 (1947); 83, 1159 (1951).

[13]C. van Trigt, Phys. Rev. 181, 97 (1969).

[14]E. M. Anderson and V. A. Zilitis, Opt. Spektrosk. 16, 177 (1964) [Opt. Spectrosc. (USSR) 16, 99 (1964)].

[15]M. Allegrini, P. Bicchi, and L. Moi, in Eighth International Conference on Atomic Physics, Göteborg, Sweden, 1982, program and abstracts, edited by I. Lindgren, A. Rosen, and S. Svanberg (Wallin and Dalholm, Lund, 1982), A88 (in press).

[16]L. D. Schearer (private communication).

[17]P. Kowalczyk, Chem. Phys. Lett. 68, 203 (1979).

[18]T. Yabuzaki, A. C. Tam, M. Hou, W. Happer, and S. M. Curry, Opt. Commun. 24, 305 (1978).

[19]V. M. Borodin and I. V. Komarov, Opt. Spektrosk. 36, 250 (1974) [Opt. Spectrosc. (USSR) 36, 145 (1974)].

[20]A. N. Klyucharev and A. V. Lazarenko, Opt. Spektrosk. 32, 1063 (1972) [Opt. Spectrosc. (USSR) 32, 576 (1972)].

[21]B. Carré, F. Roussel, P. Breger, and G. Spiess, J. Phys. B 14, 4271 (1981); 14, 4289 (1981).

[22]J. Weiner and P. Polak-Dingels, J. Chem. Phys. 74, 508 (1981).

[23]J. Krasinski, T. Stacewicz, and C. R. Stroud, Opt. Commun. 33, 158 (1980).

[24]E. A. Milne, J. London Math. Soc. 1, 1 (1926).

[25]B. P. Kibble, G. Copley, and L. Krause, Phys. Rev. 153, 9 (1967).

[26]A. C. G. Mitchell and M. W. Zemansky, *Resonance Radiation and Excited Atoms* (Cambridge University Press, Cambridge, England, 1934).